UNIVERSITY OF CAMBRIDGE

DEPARTMENT OF ENGINEERING

Stable and flexible computation in rhythmic spiking networks

Author:
Rory Byrne

Supervisor:
Prof. Tim O'Leary

I confirm that the material in this report is not copied from any published material, nor is it a paraphrase or abstract of any published material unless it is identified as such and a full source reference is given. I confirm that, other than where indicated as above, this document is my own work.

4000 words.
January 5, 2024

Abstract

The intricate balance of stability and flexibility in neural computation is a fundamental aspect of brain function, essential for both routine and adaptive behaviours. Stability is a common feature of central pattern generators, and flexibility is central to cortical function, but it is not clear how these two goals interact in a single circuit. This study investigates models of cortical gamma oscillations, and the impact of training on their rhythmicity and resilience. We find that PING networks, while capable of retaining some degree of coherence over the course of training, are not inherently more resilient to structural change than traditional asynchronous models.

Contents

1 Introduction

Animal behaviour presents an interesting paradox. On the one hand, it exhibits remarkable reliability; animals can perform highly consistent actions, from the intricate web-weaving of spiders, to the aerial acrobatics of primates, seemingly invariant to environmental conditions. On the other hand, animal behaviour is marked by its flexibility. Actions can be adjusted in subtle ways, and often in response to minute changes in sensory stimuli. This adaptability is a hallmark of higher cognition in mammals. At first glance, these two properties - stability and flexibility - seem contradictory. Stability implies a robustness to fluctuations in internal state or environmental conditions, while flexibility suggests a high degree of sensitivity to those very changes.

However, with the exception of a few speculative treatments (Yuste et al. 2005; Grillner et al. 2005), models of stability and flexibility have have taken somewhat divergent paths in small and large circuits. The study of small circuits often focuses on central pattern generators which produce specific patterns of rhythmic activity persistently. An example of this is the stomatogastric ganglion (E. Marder and Calabrese 1996), a well-studied central pattern generator, characterised by stereotyped architecture and firing patterns. The patterns produced by the STG are remarkably resilient in the face of temperature perturbations (O'Leary and Eve Marder 2016; Tang et al. 2010; Rinberg, Taylor, and Eve Marder 2013) and a 2-6 fold variation in ion channel density (Schulz, Goaillard, and Eve Marder 2006), but show limited flexibility. The multi-functionality of CPG circuits in general is dependent on neuromodulation to select between discrete patterns (Blitz and Nusbaum 2011; Stein 2009), unlikely to support the subtle variations required of fine motor control of the hand.

In contrast, the study of large circuits often shifts the focus to performance on specific memory, decision-making, or motor production tasks, where the neural system must produce the desired output and then return to rest. Here, the specific character of activity produced by the network is not a priority, and thus the emphasis is on populations of neurons that fire asynchronously (van Vreeswijk and Sompolinsky 1996), for example in the motor cortex (Churchland and Shenoy 2007; Hennequin, Vogels, and Gerstner 2014). To achieve flexibility, these cortex-dependent behaviours are often modelled using recurrent neural networks (RNNs) in the so-called "fluctuation-driven" regime (van Vreeswijk and Sompolinsky 1996). This can be thought of as a state of strong recurrent connectivity, allowing flexible variation in response to changes in inputs. However, this flexibility comes with a price, a lack of robustness to structural perturbations (Sussillo et al. 2015).

Here we aim to connect these two viewpoints by casting the stability-flexibility tradeoff as a balance between synchronous and asynchronous activity in a model of

gamma oscillations (30-100 Hz). Gamma-band activity is a hallmark of cortical processing (Han, Shapley, and Xing 2022) and is easily found in population-level recordings, but the placement of individual spikes in the cortex remains irregular (Fries 2015). In this sense, cortical activity is neither perfectly synchronous nor perfectly asynchronous, but lies in the middle. To model this balance, we initialise recurrent neural networks (RNNs) in a state of near-perfect oscillation as a PING network (Pyramidal-Interneuron Network Gamma; M. A. Whittington, Traub, and Jefferys 1995; M. A. Whittington, Stanford, et al. 1997; M. A. Whittington, Stanford, et al. 1997), and then train them to perform a discrimination task, thereby introducing task-specific asynchrony to the rhythm. This gradual shift from a predominantly synchronous state to one with controlled asynchrony is hypothesised to retain the robustness features of synchronous networks while allowing for the flexibility to perform a task.

We find that rhythmic RNNs can indeed learn a discrimination task, trading-off coherence for task performance. The drop-off in coherence is larger than expected, but remains noticeably higher than RNNs initialised in the more traditional asynchronous regime. We find that only certain subsets of the synaptic parameters need be optimised, and by optimising the inter-population synapses connecting excitatory and inhibitory units, networks can remain relatively robust to structural perturbation.

2 Results

2.1 Designing a rhythmic initial network

Prior to training a neural network, the experimenter must choose an initial state for the synaptic connection strengths (weights) in the model. The choice of initialisation can have a profound effect on the learning process, especially in spiking networks (Rossbroich, Gygax, and Zenke 2022). Two common strategies are to initialise weights with modest variance on the order $\frac{1}{N}$, giving a balanced starting point (Glorot and Bengio 2010), or to initialise weights with variance $\frac{g^2}{N}$, giving a dynamic, near-chaotic starting point for $g > 0.5$ (van Vreeswijk and Sompolinsky 1996). Here we take a third route, initialising the network to produce synchronised spiking activity at a gamma-band frequency (30-100 Hz).

In-line with prior models of gamma oscillations (M. Whittington et al. 2000), we consider a network of reciprocally-connected excitatory (E) and inhibitory (I) units. A generic description of the network's dynamics is as follows,

$$\tau \frac{dv}{dt} = f_{soma}(\mathbf{V}) + I_{app} + \sum_{I_s}^{\mathbf{D}} I_s$$

$$
\begin{aligned}
S(t) &= \mathcal{H}(v) \\
&\text{if } v > v_{th} \text{ then:} \\
&\quad \mathbf{V} = f_{reset}(\mathbf{V}) \\
\mathbf{D}_{exc} &\subseteq \{I_{IE}, I_{EE}\} \\
\mathbf{D}_{inh} &\subseteq \{I_{EI}, I_{II}\}
\end{aligned}
$$

The function f_{soma} describes the passive dynamics of the state variables $\mathbf{V}$, influenced by injected current I_{app} and a set of synaptic currents $\mathbf{D}_{exc}$ and $\mathbf{D}_{inh}$. The subscript of the synaptic current indicates the source and target population. For example, I_{IE} is the synaptic current from I units to E units. When the membrane potential reaches the threshold v_{th}, a spike is recorded and the state of the unit is reset via the function f_{reset}. The time-course of inhibitory post-synaptic currents (IPSCs) is known to be crucial for shaping the rhythm of gamma-band activity (M. Whittington et al. 2000; M. A. Whittington, Traub, Faulkner, et al. 1997), so we model each of the synaptic currents I_s dynamically:

$$
\begin{aligned}
\tau_{IE}\frac{dI_{IE}}{dt} &= -I_{IE} + W_{IE}S_I(t) \\
\tau_{EE}\frac{dI_{EE}}{dt} &= -I_{EE} + W_{EE}S_E(t) \\
\tau_{EI}\frac{dI_{EI}}{dt} &= -I_{EI} + W_{EI}S_E(t) \\
\tau_{II}\frac{dI_{II}}{dt} &= -I_{II} + W_{II}S_I(t)
\end{aligned}
$$

Such a network can produce the PING (Pyramidal-Interneuron Network Gamma) rhythm if the $E \rightarrow I$ and $I \rightarrow E$ connectivity is sufficiently strong, via a simple mechanism: applying current to the E population causes a volley of spikes, which then drives spiking in the I population. The I population in turn fires a volley of spikes, shutting down the E population. As the inhibitory post-synaptic currents (IPSCs) in E units decay, the E units will fire again, thus beginning a new cycle of the rhythm.

We constructed PING networks using the Leaky Integrate-and-Fire (LIF) model for E units and the Multi-Quadratic Integrate-and-Fire (MQIF) model (Van Pottelbergh, Drion, and Sepulchre 2018) for I units. The LIF model was defined as follows:

$$
\begin{aligned}
\tau\frac{dv}{dt} &= -(v - v_{rest}) + I_{app} + \sum_{I_s}^{\mathbf{D}} I_s \\
S(t) &= \mathcal{H}(v) \\
&\text{if } v > v_{th} \text{ then:} \\
&\quad v = v_{rest}
\end{aligned}
$$

$$\mathbf{D}_{exc} = \{I_{IE}, I_{EE}\}$$
$$\mathbf{D}_{inh} = \{I_{EI}, I_{II}\}$$

where v_{rest} is both the resting potential and the reset after a spike occurs.

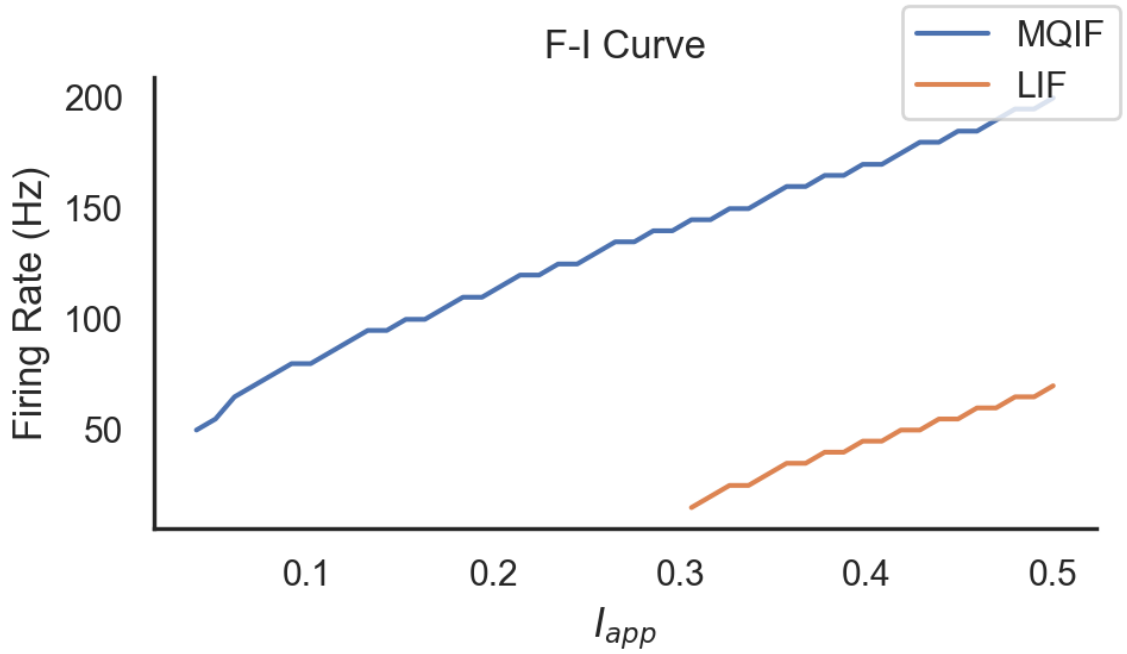

Figure 1: F-I curves for LIF and MQIF neuron models (see Table 1 and Table 2 for simulation details).

The MQIF neuron model is defined as follows,

$$\tau \frac{dv}{dt} = g_f(v - V_0)^2 - g_s(v_s - V_0^s)^2 + I_{app} + \sum_{I_s}^{\mathbf{D}} I_s$$

$$\tau_{v_s} = v - v_s$$
$$S(t) = \mathcal{H}(v)$$
if $v > v_{th}$ then:
$$v = v_{rest}$$
$$v_s = v_{rest}^s$$
$$\mathbf{D} = \{I_{EI}, I_{II}\}$$

where v is the voltage, v_s is a slow voltage-like variable capable of resonant behaviour, and g_f and g_s are the conductances of v and v_s respectively. When configured with $V_0^s < V_0$, MQIF neurons exhibit Type-2 excitability (Van Pottelbergh, Drion, and Sepulchre 2018), with a minimum firing rate of 50 Hz and high sensitivity, compared to the comparatively lower minimum firing rate of 10 Hz in the LIF model (Fig. 1). The gamma rhythm induced by resonant interneurons is more

coherent due to the dense volley of inhibitory spikes and their resulting IPSCs. This rhythm, termed RING (Resonator INduced Gamma), was found to be much more robust to perturbed inputs, relative to PING (Moca et al. 2014).

2.2 Rhythm robustness

While we felt confident about the general form of the rhythmic network, we still did not understand how they should be initialised for further training. We hypothesised that there would be a large region of parameter-space where $E \rightarrow I$ and $I \rightarrow E$ connectivity was strong enough to elicit oscillations. To explore this, we sampled $K = 625$ networks with varying $E \rightarrow I$ and $I \rightarrow E$ weights and computed a measure of oscillation coherence for each network (see Section 4), measuring the average cross-correlation of firing rates among pairs of units. Our sampling strategy was to systematically vary the parameters μ and σ of the Gaussian distribution used to sample the $E \rightarrow I$ and $I \rightarrow E$ weights.

Plotting the coherence of networks across this parameter space revealed that coherence was strong when $\mu_{E \rightarrow I} >= 0.125$ and $\mu_{I \rightarrow E} >= 0.125$ (Fig. 2). However, we were surprised to see that $\sigma_{E \rightarrow I}$ and $\sigma_{I \rightarrow E}$ have different effects on rhythm coherence. Variance in the strength of $I \rightarrow E$ synapses has little effect on the resulting rhythm, while $E \rightarrow I$ variance reduces coherence by a factor of 0.5. In some cases, strong variance in both sets of synapses degrades the rhythm entirely. We therefore opted to initialise networks with $\sigma = 0$ for both sets of weights.

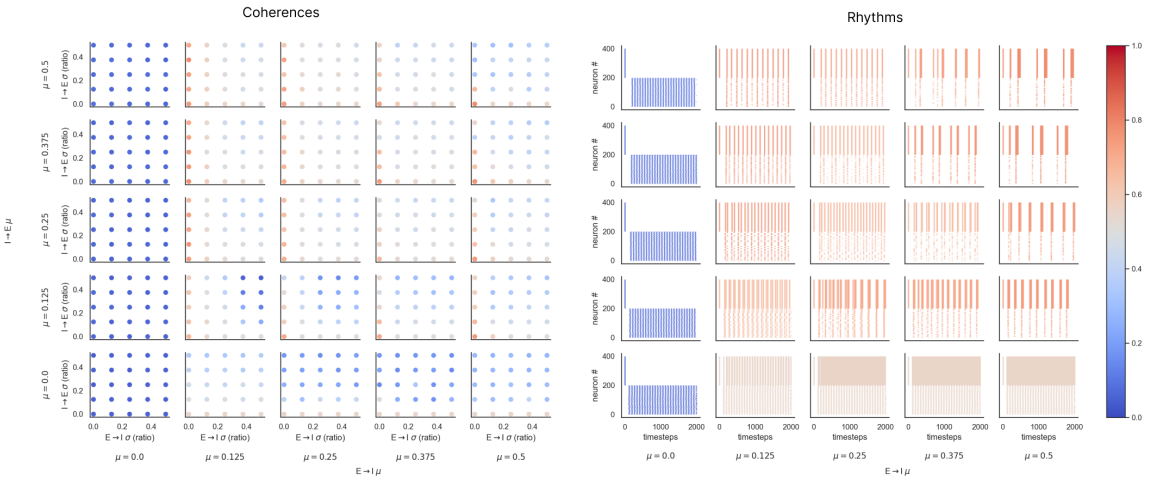

Figure 2: Robustness of gamma rhythm across $E \rightarrow I$ and $I \rightarrow E$ parameter space.

Next, we wanted to understand which parameters of the network we should optimise, so that task-specific weight changes did not disrupt the rhythm. Our hypothesis was that we should keep W_{EI} and W_{IE} fixed to maintain the structure of the rhythm, and optimise the internally-recurrent weights W_{EE} and W_{II}. To explore this, we applied increasingly large perturbations to each set of weights, then measured the

coherence of the network in response to a step current of $I_{app} = 1.0$ (Fig. 3). We found that perturbations to synapses targeting E units (W_{EE} and W_{IE}) immediately degraded coherence (green and red, dashed). Perturbations to W_{EI} (blue) had little impact because the MQIF units were already extremely sensitive to inputs (see Fig. 1), such that the entire I population typically fired simultaneously regardless of the strength of the $E \rightarrow I$ synapses. Similarly, we suspect that W_{II} (pink) synaptic perturbations had little effect because the net post-synaptic current in inhibitory units was still sufficiently strong to elicit spikes across the I population, regardless of variation in the IPSCs of I units. However, there is a sharp decline in coherence if W_{II} is perturbed enough, possibly signifying the point at which IPSCs overpower EPSCs in those units.

2.3 Scaling IPSCs increases coherence

Since variance of inputs into E units, specifically, had the largest impact on rhythm coherence, we wondered whether this could be caused by divergence in the voltages and other internal states of units during the course of the trial. As currents in E units became more heterogeneous, their participation on a beat-by-beat basis in the rhythm became more heterogeneous too, resulting in lower cross-correlation with other units in the population.

To try to equalise the internal state of E units, we opted to scale the inhibitory post-synaptic currents (IPSCs) in E units. We devised a scaling factor that varies in the range $[0, 1]$, and used it to scale IPSCs whenever spikes arrived at E units. The scaling factor, $S = \frac{v - V_{rest}}{V_{th} - V_{rest}}$, depends on the voltage of the E unit, such that the IPSC would be scaled by 1 if the unit's voltage was very close to V_{th}, and scaled by 0 if the unit was very close to rest V_{rest}. As a control, we also simulated networks where IPSCs were scaled by a constant factor of $S = 0.5$ (see Fig. 3, dotted). The net effect of this scaling was that inhibitory inputs would drive E units towards V_{rest} at every beat of the rhythm, causing them to start each new beat with similar internal states. After applying this scaling factor, the initial coherence of the network was noticeably higher (Fig. 3). This was largely due to the fact that all E units typically participated in each beat of the rhythm, leading to high scores for their cross-correlation. More interestingly, the effect of W_{IE} perturbation on coherence had qualitatively changed. Rather than a steep drop in coherence, its perturbations caused a seemingly linear decline from $C = 0.95$ to $C = 0.5$ as σ_{IE} approached 1. It was thus unclear which parameters would adversely affect coherence during training, so we decided to train networks on two subsets of synaptic parameters: intra-population (W_{EE} and W_{II}), and inter-population (W_{EI} and W_{IE}).

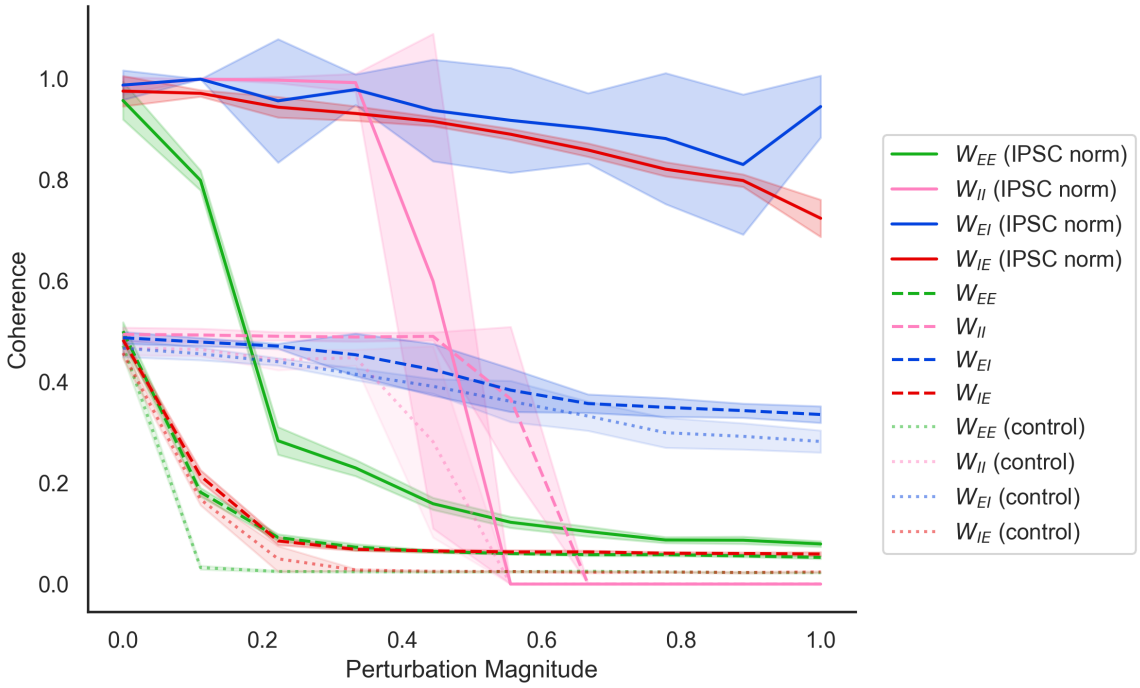

Figure 3: Coherence of gamma rhythm in response to structural perturbation. For each network type (regular, IPSC norm, control), $N = 10$ realisations were constructed, and each perturbation was repeated $K = 10$ times.

2.4 Training rhythmic networks

2.4.1 Task and network design

Having identified a suitable initialisation for rhythmic networks, we wanted to begin training on a simple discrimination task. The task is described as follows. In each trial, networks receive a static stimulus across two sensory channels $I = \{Ch_1, Ch_2\}$, and the network must learn to discriminate which of the stimuli is stronger. The stimulus is chosen from a uniform distribution, such that $Ch_1 \sim \mathcal{U}[0, 0.5]$ and $Ch_2 = 1 - Ch_1$, so that the two channels sum to 1. The target is a binary label $O = \{0, 1\}$.

The networks used a two-layer architecture mirroring the task structure. The first layer was $N = 400$ units, split into $N_{exc} = 200$ excitatory (E) units and $N_{inh} = 200$ inhibitory (I) units. The E sub-population received the stimulus as input via synaptic weights W_{SE}, and projected to the output layer via synaptic weights W_{EO}. The I units did not receive inputs or project to the output layer. The output layer comprised two Leaky-Integrator (LI) units, which are similar to the LIF units described above but without a spike-and-reset mechanism.

2.4.2 Surrogate gradients

Normally it would not be possible to use gradient-based optimisation methods on the neuron models we have described thus far, because of their discontinuous spiking mechanism. It is easy to see why: the synaptic current includes a term $I_j(t+1) = W_{ij}\mathcal{H}(v_i(t))$, where I_j is the updated current, W_{ij} is the synaptic weight from unit i to unit j, and $\mathcal{H}$ is the Heaviside function applied to pre-synaptic voltage of unit i. To assign credit to W_{ij}, the optimiser needs access to a derivative $\frac{dI_j^{syn}}{dW_{ij}}$, but this derivative depends on $\frac{d\mathcal{H}}{dv_i}$, which is undefined at the moment when the spike occurs. To get around this, a trick is used whereby the discontinuous function $\mathcal{H}$ is replaced by the a fast sigmoid function (see Section 4) during gradient computation (Zenke and Ganguli 2018; Neftci, Mostafa, and Zenke 2019; Hunsberger and Eliasmith 2015):

$$S_i(v) = \mathcal{H}(v)$$
$$\frac{dS_i}{dv} = \frac{1}{(|v|+1)^2}$$

With this simple change, it is possible to assign *approximate* credit to parameters in a spiking neural network. We say approximate because the derivative $\frac{\mathcal{H}(v)}{dv}$ is non-zero in a region around the spike threshold. Intuitively, the optimiser thinks that the neuron is communicating via a graded potential, but in reality it is emitting a discrete spike.

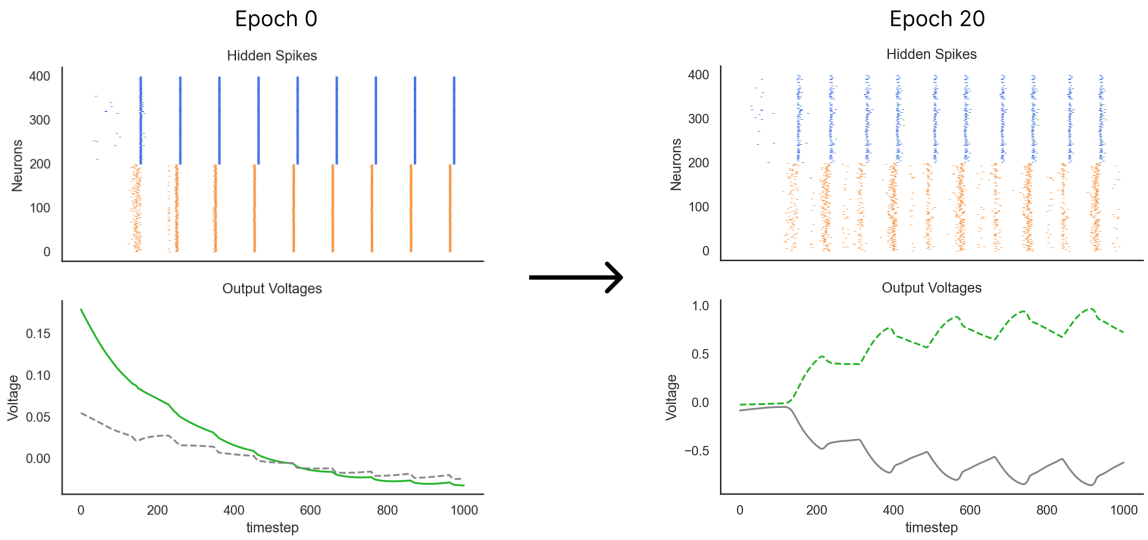

Figure 4: Spiking activity in the PING layer of the network, and voltage of the output layer, before and after training. The network was trained under the Rhythmic-Inter scheme (see Section 2.4.3)

2.4.3 Learned heterogeneity of interneurons

We also used the surrogate trick in a second part of our model: to add heterogeneity to the population of interneurons. One of our primary goals was to introduce asynchrony into the initially-synchronous activity produced by the network. However, due to the low rheobase of MQIF units (Fig. 1), IPSCs of a purely MQIF I population imposed quite a strong constraint on when E units could fire. To allow for more flexibility, we assigned a scalar value k_i to each interneuron i, which would determine its "type", and then optimised the vector $\vec{k}$ during training. The k values were used to switch the neuron dynamics between MQIF and the less excitable LIF.

We defined $K_i = \mathcal{H}(k_i)$, where $\mathcal{H}$ represents the Heaviside step function, similar to the activation function used to simulate spiking in the neuron models. This binary value K_i allowed us to switch the neuron's dynamics discretely during forward simulation:

$$v_i^{t+1} = v_i^t + (K_i * f_{MQIF}(\mathbf{V}) + (1 - K_i) * f_{LIF}(\mathbf{V}))$$

where v_i^t is the voltage of unit i at time step t, and $f_{MQIF}(\mathbf{V})$ and $f_{LIF}(\mathbf{V})$ represent the state update functions of the MQIF and LIF units respectively, applied to state variables $\mathbf{V}$.

Crucially, during the backwards pass, gradients are computed using a fast-sigmoid derivative $\frac{1}{(|k_i|+1)^2}$, rather than $\frac{d\mathcal{H}}{dk_i}$. This substitution means that the optimiser perceives the voltage update step to be a linear combination of the MQIF and LIF updates, and tries to find the optimal weighting between them. In the forward simulations, however, a discrete choice is made using $\mathcal{H}$.

2.4.4 Trading coherence for performance

To understand how learning differs in rhythmic versus asynchronous networks, we trained sets of networks from both rhythmic and asynchronous initialisations. To maintain rhythm coherence during the course of training, we wanted to optimise as few of the weights as possible. Our hypothesis was that keeping W_{EI} and W_{IE} fixed would preserve the PING mechanism, allowing us to optimise W_{EE} and W_{II} for the task. However, our earlier results suggest that the coherence of the rhythm is more sensitive to W_{EE} and W_{II}, so those parameters might not be the best candidates for optimisation. We therefore decided to compare the asynchronous initialisation with two training regimes of rhythmic networks: Intra-Population Inter-Population. Here, intra-population refers to training the recurrent weights of each population (W_{EE} and W_{II}), while inter-population trains the weights that connects populations (W_{EI} and W_{IE}). Asynchronous networks were initialised in a "fluctuation-driven regime" (van Vreeswijk and Sompolinsky 1996), and both forms of rhythmic network were initialised with $W_{EI} = 0.125$, $W_{IE} = 0.5$, and $W_{EE} = W_{II} = 0$. The full

initialisation scheme is described in Table **??**.

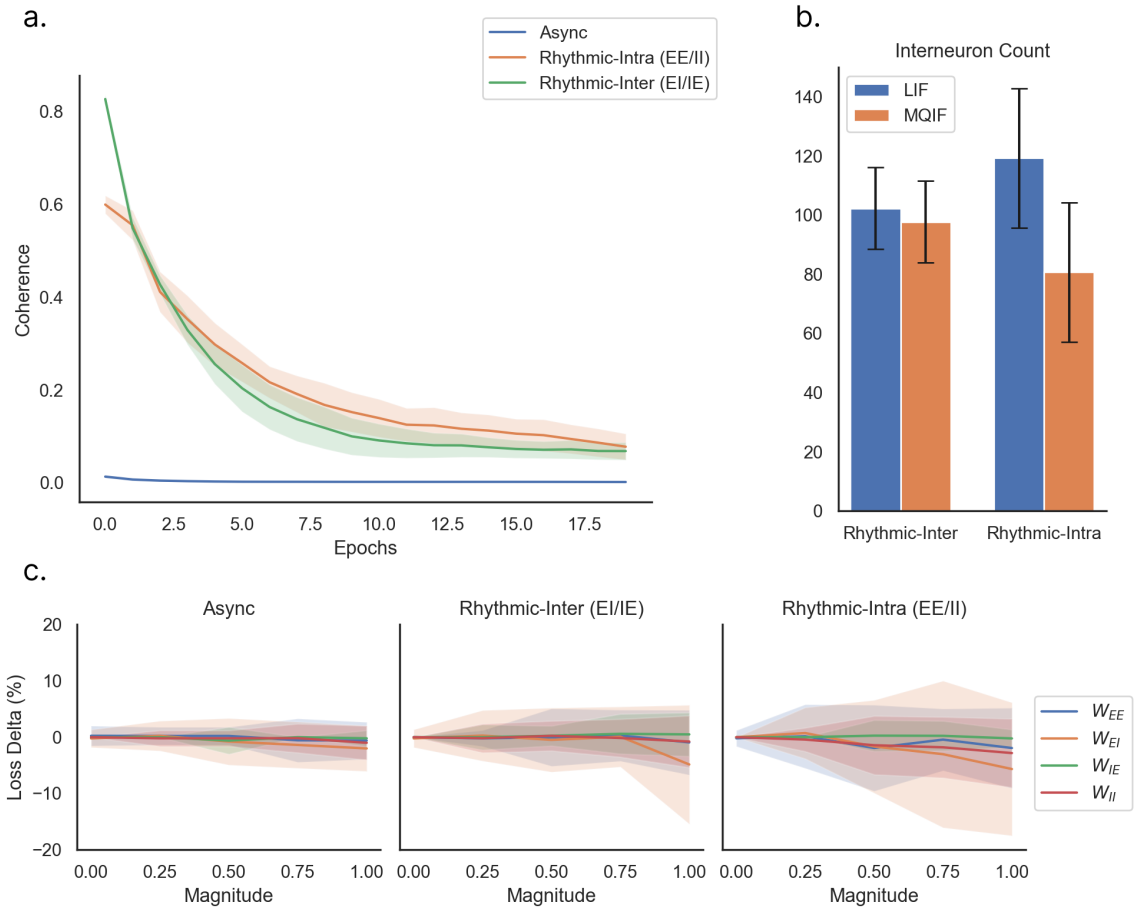

Figure 5: Analysis of trained networks. a) evolution of activity coherence over the course of 20 epochs of training. b) Learned distribution of MQIF and LIF neurons among the I population, error bars signify standard deviation. c) Effect of structural perturbation on classification accuracy. Each network was realised and trained 10 times, and each perturbation was then applied 10 times, giving 100 perturbations per-weight matrix (400 total). Error represents standard deviation.

We trained 10 realisations of each network and measured the coherence over the course of training (Fig. 5 a.). Coherence of networks declined significantly over $E = 20$ epochs, indicating that spike timings and the participation of units in the rhythm were becoming more irregular. Coherence reached a plateau after around 15 epochs, but remained noticeably higher than the asynchronous networks (Fig. 5). Coherence decay was similar for the Rhythmic-Inter and Rhythmic-Intra networks but networks where local recurrence was trained (W_{EE} and W_{II}) were marginally more coherent. This was surprising, because our earlier perturbation simulation suggested that changes to W_{EE} would have a strong detrimental effect on coherence. Perhaps this is because the structure of weights learned by the optimiser is different

to the Gaussian-distributed weights used in our robustness analysis.

Neural circuits, in both biological and neuromorphic contexts (Benjamin et al. 2014), are subject to various forms of perturbation. If there is a phylogenetic link between CPGs and cortical circuits (Grillner et al. 2005) then we would expect cortical circuits to share some of the resilience of CPGs, such as robustness to structural change. To simulate this, we systematically perturbed synaptic weights of the asynchronous, rhythmic (inter), and rhythmic (intra) networks that were trained. The perturbation was applied independently to each set of weights (see Section 4 for details), and the change in classification accuracy was plotted as a function of perturbation magnitude (Fig. 5). Surprisingly, we found that the asynchronously-initialised networks were more robust than rhythmic networks. However, rhythmic networks with inter-population training were slightly more coherent than those where internal recurrence was optimised. This is consistent with the hypothesis that the synchrony conferred by the PING rhythm is in-fact more fragile than traditional asynchronous activity of RNNs.

3 Discussion

The possibility that cortical circuitry retains essential features found in smaller circuits is a tantalising one. The results of our study suggest that inhibition-constrained rhythms, as observed both in CPGs and cortical circuits, are not incompatible with task-driven learning. However, our findings also indicate that the mere presence of such rhythmically constrained activity in cortical circuits does not automatically confer the same level of robustness typically attributed to smaller CPG circuits.

This leads us to an important realisation: connectivity motifs, while crucial, may not be sufficient in themselves to achieve the intricate balance of stability and flexibility required for complex computational tasks. The role of cellular mechanisms, particularly nonlinear aspects such as conductance densities (O'Leary and Eve Marder 2016), is likely a vital piece of the puzzle. These intracellular factors play a significant role in modulating neural responses and, by extension, the overall behaviour of the network. In recent years, the rise of deep learning and connectionist modeling has brought significant attention to the patterns of connectivity within neural networks. While these models have undeniably advanced our understanding of neural computation, there is a risk that they may obscure the critical role played by intracellular mechanisms.

Our study highlights the need to integrate a deeper understanding of cellular processes with our knowledge of network connectivity. Spiking neural networks like the kind presented here are a good opportunity to do this, by introducing cellular heterogeneity (Perez-Nieves et al. 2021) alongside the connectivity patterns discovered

by optimisation.

4 Methods

4.1 Neuron Types

Two different neuron models were used for the excitatory (E) and inhibitory (I) populations. For the E population, Leaky Integrate-and-Fire (LIF) units were used with typical biophysical configuration Table 1. For the I population, Multiple-Quadratic Integrate-and-Fire (MQIF) units were configured for Type-2 excitability (Van Pottelbergh, Drion, and Sepulchre 2018), summarised in Table 2. In some experiments, the I population was a mixture of MQIF and LIF units.

Parameter	Value
V_{th}	-55 mV
V_{reset}	-70 mV
τ	10 ms

Table 1: LIF Parameters

Parameter	Value
C	1 ms
g_f	0.8
g_s	1.5
V_{th}	-55 mV
V_0	-70 mV
V_0^s	-71 mV
V_{reset}	-70 mV
V_{reset}^s	-66 mV

Table 2: MQIF Parameters for Type-II excitability

The LIF and MQIF units were simulated using the Euler integration method, a first-order method yielding the following update rule for the LIF model:

$$v^{t+1} = v^t + (\frac{\Delta t}{\tau}) * (-(v^t - v_{rest}) + I_{app}^t + \sum_x^{I_S} I_s^t) \tag{1}$$

and similarly for the MQIF model:

$$v^{t+1} = v^t + (\frac{\Delta t}{\tau_v}) * (g_f(v - V_0)^2 - g_s(v - V_0^s)^2 + I_{app}^t + \sum_x^{I_S} I_s^t) \tag{2}$$

$$v_s^{t+1} = v_s^t + (\frac{\Delta t}{\tau_{v_s}}) * (v - v_s) \tag{3}$$

While the Euler method is less accurate than higher-order integration methods, its local truncation error is proportional to Δt^2. In our simulations a small $\Delta t = 0.1$ ms is used to accurately capture sub-threshold dynamics in MQIF units, leading to a very small error bound in practice.

4.2 Network Connectivity

		Async	**Rhythmic-Inter**	**Rhythmic-Intra**
W_{SE}	μ	0.8	0.8	0.8
	σ	0.0	0.0	0.0
W_{EE}	μ	0.2	0.0	0.0
	σ	0.1	0.0	0.0
W_{EI}	μ	0.2	0.125	0.125
	σ	0.1	0.8	0.8
W_{II}	μ	0.2	0.0	0.0
	σ	0.1	0.0	0.0
W_{IE}	μ	0.2	0.5	0.5
	σ	0.1	0.0	0.0
W_{EO}	μ	0.0	0.0	0.0
	σ	0.01	0.01	0.01
W_{IO}	μ	0.0	0.0	0.0
	σ	0.01	0.01	0.01

Table 3: Network initialisations

We constructed networks of $N_{exc} = 200$ excitatory units and $N_{inh} = 200$ inhibitory units. This gives four sets of synaptic connections between and within the subpopulations with weights W_{IE}, W_{EE}, W_{EI}, and W_{II}. Each set of synaptic weights is drawn from a separate normal distribution, summarised in (Table **??**).

4.3 Measuring oscillation coherence

Oscillation coherence was measured as the average pair-wise cross-correlation of firing rates, using a Gaussian filter $G(t)$:

$$C = \frac{2}{N(N-1)} \sum_{i=1}^{N-1} \sum_{j=i+1}^{N} \int_{-\infty}^{\infty} (S_i(t) * G(t)) \cdot (S_j(t-\tau) * G(t-\tau)) dt \tag{4}$$

$$G(t) = \frac{1}{\sigma\sqrt{2\pi}} e^{-\frac{t^2}{2\sigma^2}} \tag{5}$$

4.4 Training procedure

The output of the network was taken to be the voltage values of the output units at the final timestep of the simulation, a $B \times 2$ matrix V, where $B = 128$ is the batch size. The softmax function to convert the final voltages into a probability distribution (positive values, summing to 1), before being compared to class labels C, a $B \times 1$ matrix, to compute the cross-entropy loss function:

$$\mathcal{L}_{\text{total}}(V, C) = -\frac{1}{B} \sum_{o=1}^{B} \sum_{c=1}^{M} y_{o,c} \log \left(\frac{e^{V_{o,c}}}{\sum_{k=1}^{M} e^{V_{o,k}}} \right)$$

All networks were trained for $E = 10$ epochs, typically resulting in accuracy over 85%. Accuracy was typically reported as the percentage of trials correctly labeled in the batch, rather than loss, because different model instantiations and neuron types have different abilities to create divergent voltages in the output layer (more divergence results in lower cross-entropy loss). For each parameter regime, we trained 10 networks and took the mean accuracy over the population of networks.

Parameter	Value
Epochs	10
Learning Rate	0.005
Batch Size	128
Δt	0.0001
Duration	1000

Table 4: very basic table

4.5 Structural Perturbation

Following from (Sussillo et al. 2015), we perturbed weight matrices by adding Gaussian noise element-wise. The perturbation was done separately for each weight matrix W, such that $W_{ij} \leftarrow W_{ij} + \beta_{ij}$ where β was Gaussian noise. To produce (Fig. 5), we trained $N = 10$ realisations of each network and repeated the perturbation process 10 times for each weight matrix in the network, giving a total of $S = 100$ perturbed accuracy deltas for each weight matrix. We plotted the mean accuracy delta and the standard deviation of the accuracy deltas across all 100 perturbations.

References

Whittington, Miles A., Roger D. Traub, and John G. R. Jefferys (Feb. 1995). "Synchronized Oscillations in Interneuron Networks Driven by Metabotropic Glutamate Receptor Activation". In: *Nature* 373.6515, pp. 612–615. ISSN: 1476-4687. DOI: 10.1038/373612a0. (Visited on 12/31/2023).

Marder, E. and R. L. Calabrese (July 1996). "Principles of Rhythmic Motor Pattern Generation". In: *Physiological Reviews* 76.3, pp. 687–717. ISSN: 0031-9333. DOI: 10.1152/physrev.1996.76.3.687. (Visited on 09/08/2023).

van Vreeswijk, C. and H. Sompolinsky (Dec. 1996). "Chaos in Neuronal Networks with Balanced Excitatory and Inhibitory Activity". In: *Science* 274.5293, pp. 1724–1726. DOI: 10.1126/science.274.5293.1724. (Visited on 01/03/2024).

Whittington, Miles A., Ian M. Stanford, et al. (1997). "Spatiotemporal Patterns of γ Frequency Oscillations Tetanically Induced in the Rat Hippocampal Slice". In: *The Journal of Physiology* 502.3, pp. 591–607. ISSN: 1469-7793. DOI: 10.1111/j.1469-7793.1997.591bj.x. (Visited on 12/31/2023).

Whittington, Miles A., Roger D. Traub, Howard J. Faulkner, et al. (Oct. 1997). "Recurrent Excitatory Postsynaptic Potentials Induced by Synchronized Fast Cortical Oscillations". In: *Proceedings of the National Academy of Sciences* 94.22, pp. 12198–12203. DOI: 10.1073/pnas.94.22.12198. (Visited on 12/31/2023).

Whittington, M.A et al. (Dec. 2000). "Inhibition-Based Rhythms: Experimental and Mathematical Observations on Network Dynamics". In: *International Journal of Psychophysiology* 38.3, pp. 315–336. ISSN: 01678760. DOI: 10.1016/S0167-8760(00)00173-2. (Visited on 09/15/2023).

Grillner, Sten et al. (Oct. 2005). "Microcircuits in Action – from CPGs to Neocortex". In: *Trends in Neurosciences* 28.10, pp. 525–533. ISSN: 0166-2236, 1878-108X. DOI: 10.1016/j.tins.2005.08.003. (Visited on 01/03/2024).

Yuste, Rafael et al. (June 2005). "The Cortex as a Central Pattern Generator". In: *Nature Reviews Neuroscience* 6.6, pp. 477–483. ISSN: 1471-0048. DOI: 10.1038/nrn1686. (Visited on 01/03/2024).

Schulz, David J., Jean-Marc Goaillard, and Eve Marder (Mar. 2006). "Variable Channel Expression in Identified Single and Electrically Coupled Neurons in Different Animals". In: *Nature Neuroscience* 9.3, pp. 356–362. ISSN: 1546-1726. DOI: 10.1038/nn1639. (Visited on 05/04/2023).

Churchland, Mark M. and Krishna V. Shenoy (June 2007). "Temporal Complexity and Heterogeneity of Single-Neuron Activity in Premotor and Motor Cortex". In: *Journal of Neurophysiology* 97.6, pp. 4235–4257. ISSN: 0022-3077. DOI: 10.1152/jn.00095.2007. (Visited on 02/06/2022).

Stein, Wolfgang (Nov. 2009). "Modulation of Stomatogastric Rhythms". In: *Journal of Comparative Physiology A* 195.11, pp. 989–1009. ISSN: 1432-1351. DOI: 10.1007/s00359-009-0483-y. (Visited on 01/03/2024).

Glorot, Xavier and Yoshua Bengio (Mar. 2010). "Understanding the Difficulty of Training Deep Feedforward Neural Networks". In: *Proceedings of the Thirteenth International Conference on Artificial Intelligence and Statistics*. JMLR Workshop and Conference Proceedings, pp. 249–256. (Visited on 01/01/2024).

Tang, Lamont S. et al. (Aug. 2010). "Precise Temperature Compensation of Phase in a Rhythmic Motor Pattern". In: *PLOS Biology* 8.8, e1000469. ISSN: 1545-7885. DOI: 10.1371/journal.pbio.1000469. (Visited on 01/05/2024).

Blitz, Dawn M and Michael P Nusbaum (Aug. 2011). "Neural Circuit Flexibility in a Small Sensorimotor System". In: *Current Opinion in Neurobiology*. Sensory and Motor Systems 21.4, pp. 544–552. ISSN: 0959-4388. DOI: 10.1016/j.conb.2011.05.019. (Visited on 12/30/2023).

Rinberg, Anatoly, Adam L. Taylor, and Eve Marder (Jan. 2013). "The Effects of Temperature on the Stability of a Neuronal Oscillator". In: *PLOS Computational Biology* 9.1, e1002857. ISSN: 1553-7358. DOI: 10.1371/journal.pcbi.1002857. (Visited on 01/05/2024).

Benjamin, Ben Varkey et al. (May 2014). "Neurogrid: A Mixed-Analog-Digital Multichip System for Large-Scale Neural Simulations". In: *Proceedings of the IEEE* 102.5, pp. 699–716. ISSN: 1558-2256. DOI: 10.1109/JPROC.2014.2313565. (Visited on 11/15/2023).

Hennequin, Guillaume, Tim P. Vogels, and Wulfram Gerstner (June 2014). "Optimal Control of Transient Dynamics in Balanced Networks Supports Generation of Complex Movements". In: *Neuron* 82.6, pp. 1394–1406. ISSN: 0896-6273. DOI: 10.1016/j.neuron.2014.04.045. (Visited on 11/27/2021).

Moca, Vasile V. et al. (Jan. 2014). "Membrane Resonance Enables Stable and Robust Gamma Oscillations". In: *Cerebral Cortex* 24.1, pp. 119–142. ISSN: 1047-3211. DOI: 10.1093/cercor/bhs293. (Visited on 11/19/2023).

Fries, Pascal (Oct. 2015). "Rhythms for Cognition: Communication through Coherence". In: *Neuron* 88.1, pp. 220–235. ISSN: 0896-6273. DOI: 10.1016/j.neuron.2015.09.034. (Visited on 01/05/2024).

Hunsberger, Eric and Chris Eliasmith (Oct. 2015). *Spiking Deep Networks with LIF Neurons*. DOI: 10.48550/arXiv.1510.08829. arXiv: 1510.08829 [cs]. (Visited on 01/01/2024).

Sussillo, David et al. (July 2015). "A Neural Network That Finds a Naturalistic Solution for the Production of Muscle Activity". In: *Nature Neuroscience* 18.7, pp. 1025–1033. ISSN: 1546-1726. DOI: 10.1038/nn.4042. (Visited on 10/20/2021).

O'Leary, Timothy and Eve Marder (Nov. 2016). "Temperature-Robust Neural Function from Activity-Dependent Ion Channel Regulation". In: *Current Biology* 26.21, pp. 2935–2941. ISSN: 0960-9822. DOI: 10.1016/j.cub.2016.08.061. (Visited on 12/29/2023).

Van Pottelbergh, Tomas, Guillaume Drion, and Rodolphe Sepulchre (Apr. 2018). "Robust Modulation of Integrate-and-Fire Models". In: *Neural Computation* 30.4, pp. 987–1011. ISSN: 0899-7667, 1530-888X. DOI: 10.1162/neco_a_01065. arXiv: 1709.06824 [q-bio]. (Visited on 08/12/2023).

Zenke, Friedemann and Surya Ganguli (June 2018). "SuperSpike: Supervised Learning in Multilayer Spiking Neural Networks". In: *Neural Computation* 30.6, pp. 1514–1541. ISSN: 0899-7667. DOI: 10.1162/neco_a_01086. (Visited on 02/07/2022).

Neftci, Emre O., Hesham Mostafa, and Friedemann Zenke (Nov. 2019). "Surrogate Gradient Learning in Spiking Neural Networks: Bringing the Power of Gradient-

Based Optimization to Spiking Neural Networks". In: *IEEE Signal Processing Magazine* 36.6, pp. 51–63. ISSN: 1558-0792. DOI: 10.1109/MSP.2019.2931595.

Perez-Nieves, Nicolas et al. (Oct. 2021). "Neural Heterogeneity Promotes Robust Learning". In: *Nature Communications* 12.1, p. 5791. ISSN: 2041-1723. DOI: 10.1038/s41467-021-26022-3. (Visited on 02/07/2022).

Han, Chuanliang, Robert Shapley, and Dajun Xing (Aug. 2022). "Gamma Rhythms in the Visual Cortex: Functions and Mechanisms". In: *Cognitive Neurodynamics* 16.4, pp. 745–756. ISSN: 1871-4099. DOI: 10.1007/s11571-021-09767-x. (Visited on 11/02/2023).

Rossbroich, Julian, Julia Gygax, and Friedemann Zenke (Dec. 2022). "Fluctuation-Driven Initialization for Spiking Neural Network Training". In: *Neuromorphic Computing and Engineering* 2.4, p. 044016. ISSN: 2634-4386. DOI: 10.1088/2634-4386/ac97bb. (Visited on 01/05/2024).